

# Detection of Pediatric Pneumonia Based on Chest X-Ray Image Using Extraction Method

1<sup>st</sup> Eva Rianti

Department of Information System  
Universitas Putra Indonesia YPTK  
Padang, Indonesia  
evarianti@upiyptk.ac.id

2<sup>nd</sup> Iskandar Fitri

Department of Information Technology  
Universitas Putra Indonesia YPTK  
Padang, Indonesia  
if@upiyptk.ac.id

3<sup>rd</sup> Sumijan

Department of Information Technology  
Universitas Putra Indonesia YPTK  
Padang, Indonesia  
sumijan@upiyptk.ac.id

**Abstract**—Early diagnosis of pneumonia in children (pediatric) is critical to ensure curative treatment and increase survival rates. Chest X-ray images stand out as the most frequently used method for the diagnosis of pneumonia. Currently, computational tools mainly focus on assessing adult pneumonia, which poses challenges for assessing pneumonia in children, especially infants. This research begins with the preprocessing stage, which includes converting the input image from RGB to Grayscale, followed by automatic image enhancement and cropping. Next, segmentation techniques are used, which involve thresholding, opening, image inversion, boundary cleaning, closing, filtering, image filling, and image reduction. The results of the segmentation process then go to the extraction stage, where the entity processed is the image texture value that comes from the segmentation results. From the research results were obtained using 60 lung X-Ray images. X-ray images of children as test data. This study was successful in detecting 28 true positive (TP) lung X-Ray images and 29 true negative (TN) images. Meanwhile, the results of false negative (FN) detection were 2 images and false positive (FP) were 1 images, so the accuracy in this study was 95%.

**Keywords**—X-Ray Images, Ekstraktion, Pediatric Pneumonia, GLCM, SVM

## I. INTRODUCTION

It provides several advantages to the medical field through information technology in its digital image processing that is derived from various medical modalities such as X-rays, CT scans, and MRIs [1]. These advancements have greatly improved the performance of medical image analysis in radiological examinations [2]. Of all the radiological examinations practiced, the role of X-rays is of paramount consideration [3]. X-ray examinations are routinely used in the production of images of the heart [4], lungs [5], respiratory tract [6], blood vessels [7], and lymph nodes [8, [9]. Chest X-rays are principally used to establish diseases of infections of the lungs, such as pneumonia, which is a form of acute respiratory infection in the lungs.

Pneumonia is an acute infection of the respiratory system that may involve one or both lungs due to infection by bacteria, viruses, or even fungi in the air [11]. On the contrary, pneumonia spreads through mediums of air via coughing or sneezing, through blood transmission, namely during or soon after birth, and on contact with a contaminated surface [12]. Though the normal immune system keeps these infectious agents at bay, several factors can attenuate this defense. Early detection and treatment can substantially decrease childhood mortality due to pneumonia [13]. Childhood pneumonia is difficult to diagnose because of the low sensitivity of microbiological tests and nonspecific clinical manifestations. A chest X-ray will be a paramount and prevalent diagnostic technique that gives a very simple, efficient way for physicians to review the internal organs. However, interpreting chest X-rays requires a radiologist's expertise to

make accurate diagnoses and provide effective medical interventions.

Currently, the computational tools are focused on the assessment of pneumonia in adults, thus posing challenges in the diagnosis of paediatric pneumonia [14], [15], especially in infants [16], [17]. In this research, different methods are practised to provide accuracy towards the diagnosis of Childhood pneumonia by assessing the chest X-ray results. However, there's no proposition made for the routine use of chest radiography for the diagnosis of Childhood Pneumonia in an out-patient setting [18].



Fig. 1. Left, Chest X-Ray Normal, Right Chest X-Ray Pneumonia

Pneumonia causes several pathological conditions, such as pleural effusion, which is an abnormal collection of fluid in the lungs and can cause respiratory distress. Diagnosis of pneumonia at the earliest stage of onset is the key to instituting curative interventions that increase survival chances. Imaging modalities used in the diagnosis of pneumonia essentially remain chest X-ray imaging. There is, therefore, a clear imperative for an automated system tailored toward the detection of pneumonia.

Antecedent research by Mahedi Masud in 2021 [19] underscored the serious consequences of pneumonia, which alone causes almost one-fifth of the mortality of children worldwide. The advanced mortality rate of most developing countries is mainly due to the lack of appropriate diagnostic facilities on time. Inclusion of machine learning-based diagnosis procedures therefore becomes a crucial lead-time and low-cost method for pneumonia diagnosis. In this research, a new approach is being suggested for the diagnosis and subtyping of pneumonia through an analysis of chest radiographs (X-rays). The analysis considers extracting two sets of complementary chest X-ray features from images. This paper presents a new methodology for the diagnosis of pneumonia that places special emphasis on the diversification of information derived from a chest radiograph and their subsequent fusions for classification using an ensemble learning algorithm. Noticeable results demonstrate an accuracy of 86.30% in classification. Looking ahead to future work, it is envisioned that the integration of similar chest X-ray datasets in further research studies may lead to the development of higher-accuracy diagnostic methods.

A 2023 research paper by Natali Barakat [10] explores a machine-learning approach applied to chest X-rays for the detection of pediatric pneumonia. The paper deals with the

automation of the early detection of pediatric pneumonia using machine learning and explicitly dwells on its computational efficiency in contrast to deep learning methods. The proposed method requires data augmentation for the handled datasets to overcome class imbalances and for the fine-tuning of feature extraction methods as well as for the evaluation of various machine learning models' performance. At the pre-processing stage, complete images will be standardized to have a common size, and the images will be changed into gray scale. AlexNet will be used since it offers the capability of performing high-level image classification for pneumonia. The next step is to extract sixteen statistical features from each chest X-ray image, followed by feature value normalization so that all of them will be scaled within the range 0 to 1. This work only restricts itself to binary classification of the pneumonia using pediatric X-rays with certain resolution criteria and a sufficient number of samples. It is explained, in the light of previous studies, that the future development in detecting childhood pneumonia through digital image processing is needed significantly and opens ways for future research.

Development in potential digital image processing focused on pediatric pneumonia will have the potential to bring the best results with more precision. This development

in the field of digital image processing focuses on the improvement in texture extraction to identify children's pneumonia [21]. A new texture extraction process is conceptualized through the refinement of the Gray Level Co-Occurrence Matrix algorithm model [22]. This uniquely designed algorithmic model is aimed at executing the extraction process relevant to the identification of childhood pneumonia in chest X-ray images [23]. It is envisaged that the evolved texture extraction process aspires to garner optimal textural characteristics crucial for precise identification of childhood pneumonia. As Image processing techniques have evolved with changing times, with a changing algorithm model of the GLCM within this research, it is expected to give heightened identification accuracy.

## II. METHODOLOGY

### A. Framework Research

This research was conducted to increase the quality of X-ray images in identifying childhood pneumonia by applying the texture extraction method using the GLCM algorithm. It is envisioned to aid hospitals in rapidly and accurately detecting areas of the lungs infected by the disease. Figure 1 below shows the framework of the research:

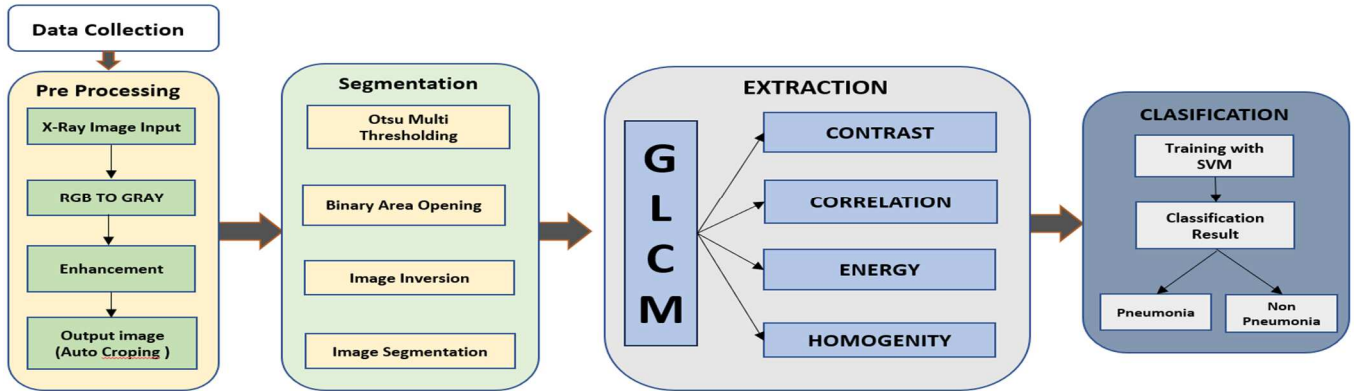


Fig. 2. Framework Research

### B. Framework Research Details

#### 1) Data Collection

Data collection involves the X-ray images captured from the SIEMENS MULTI SELECT DR X-Ray machine. The data collection for the study is conducted at the Radiology section of the Regional General Hospital, Dr. Rasidin, Padang City. The acquired X-ray images will show a sense of alteration pulmonary conditions of the pneumonia-ill children when some additional X-ray images show different lung diseases.

#### 2) Pre-Processing

There are some importance steps in preprocessing, starting from the image acquisition phase to the very primary input, followed by a grayscale image, noise filtering, and lastly creating a binary image. Besides, advanced preprocessing is also a process that can normalize images and prevent influences on colored [24], texture [25], intensity, and important information [26]. In the following research, several pre-processing stages have been performed, including as the input of X-ray data, the subsequent image processing step-by-step from RGB to grayscale, then enhancement, until cropping procedures.

a) *Chest X-ray Image Input*: The image input involves the acquisition or procurement of the x-ray image of the pediatric lungs. This whole process initiates after data categorization, where the data is categorized according to the x-ray images of the children lungs, particularly those suffering from pneumonia, alongside other different x-ray images indicating other lung diseases.

b) *RGB to Grayscale*: That is, the first process in the pre-processing stage is the conversion of the original image from its default image type, RGB, into gray scale [27]. It is carried out to reduce the color form of the original image [28], and consequently the intensity values of its pixels represent the gray scale [29].

c) *Enhancement*: Algorithmic enhancement refers to the systematic refinement or optimization of previously conducted stages, aiming to enhance overall performance, efficiency, and specific features [30]. The primary objective of an enhancement algorithm is to yield superior, expedited, and tailored outcomes to meet specific requirements [31]. The enhancement stage in this context seeks to augment the separation between intensity values within the data,

facilitating the attainment of improved image quality more suitable for subsequent stages. In the course of this study, enhancement procedures were instituted due to several factors, encompassing the presence of noise in the X-ray image, inadequate image brightness or excessive brightness, and blurriness in the X-ray image.

*d) Cropping:* The cropping stage is designed to diminish the dimensions of the image by strategically truncating it at specific coordinates within the image area. This process involves excising portions of the image, thereby eliminating extraneous elements to obtain sections of the image with predetermined dimensions. The objective of this cropping procedure is to accentuate the primary object within the image by isolating and emphasizing specific regions, thus enhancing the prominence of the main object.

### 3) Segmentation

Segmentation is the intricate process of partitioning an image into multiple smaller components. The primary objective of image segmentation lies in delineating the boundaries or contours of objects, demarcating objects from the background, and categorizing image pixels into distinct groups based on specific characteristics such as color, intensity, texture, or shape. In this research endeavor, several sequential stages are undertaken to yield the desired segmentation outcomes for the targeted object. The segmentation stage is initiated with the utilization of the pre-processed cropped image. Subsequent stages, including Otsu multi-thresholding, binary area opening, image inversion, border clearing, morphology closing, object filtering, image filling, and binary area opening, are systematically executed to obtain segmentation results aligning with the research objectives.

*a) Otsu Multi Thresholding:* This stage is executed to achieve image segmentation at multiple threshold levels, surpassing the typical binary segmentation. The objective is to autonomously compute optimal thresholds, effectively segregating objects from the background in binary images characterized by two threshold levels. In the context of this research, the images under consideration exhibit more than two groups of pixels, prompting the need for classification into distinct classes based on intensity or specific features.

*b) Binary Area Opening:* This stage is implemented to achieve image segmentation employing multiple threshold levels. In this research, the binary opening stage is employed to eliminate small components or objects within the image that underwent prior processing through Otsu Multi-Thresholding. The primary objective is to retain the larger components while effectively removing smaller ones.

*c) Image Inversion:* Image inversion is executed during the segmentation stage of this research to accentuate image features that might be compelling to discern in the original image. This process involves altering the previously processed image within the binary opening area. The objective of image inversion at this stage is to enhance contrast, thereby rendering even minuscule features within the radiology image distinctly visible.

*d) Image Segmentation:* At this stage, the segmentation process is initiated utilizing the image subtraction outcomes to partition the image into distinct segments predicated on specific characteristics. In this study, the segmentation

process focuses on the texture of the X-ray image of the pediatric lungs as the defining characteristic.

### 4) Extraction Result

Image extraction is the process of retrieving important information or features from a digital image for the purpose of analysis and further processing. The purpose of image extraction is to reduce the dimensions of image data and describe relevant information from the image. The image extraction used in this research is texture feature extraction.

*a) Texture Feature Extraction:* Texture feature extraction is a process that describes the textural properties of an image. The purpose of texture features is to identify patterns, structures, or texture characteristics in images. There are several methods commonly used for extracting texture features from images. In this research, the extraction texture used was GLCM (Gray-Level Co-occurrence Matrix).

*b) GLCM (Gray-Level Co-occurrence Matrix):* In the GLCM process, the current stage involves computing the frequency of pixel intensity pair occurrences at a specified distance and direction. In the context of this research, GLCM serves to extract features encompassing entropy, contrast, correlation, and energy.

- *Contrast:* This stage is employed for delineating texture patterns within digital images. Contrast quantifies the degree of disparity in brightness levels between adjacent pairs of pixels in an image. Elevated contrast values signify numerous abrupt shifts in pixel intensities, whereas diminished contrast values indicate the prevalence of smoother or more homogeneous texture patterns in the image.
- *Correlation:* Correlation is intended to gauge the linear association between the gray intensity of pixels within an image, offering *insights* into pixels that exhibit a linear relationship in terms of gray intensity within the image.
- *Energy:* In image processing, the concept of energy is employed to compute an intensity measure reflecting the even distribution of gray values throughout the image. A higher energy value indicates a more dispersed or less concentrated gray intensity within the image. Conversely, a lower energy value suggests the aggregation or concentration of gray intensity in the image, indicative of a more homogeneous or smooth texture.
- Homogeneity in digital image processing aims to measure the gray intensity of adjacent pixels in an image that tend to be similar or homogeneous. The higher the homogeneity value, the more similar or homogeneous the gray intensity in the image, which can describe a smoother or more consistent texture. On the other hand, if the homogeneity value of the resulting image is low, the resulting variation will be greater in gray intensity and the image texture will be rougher.

### 5) Classification: Support Vector Machine (SVM)

Classification denotes the systematic categorization of images into specific groups contingent upon discernible characteristics. The primary objective of image classification is to enhance comprehension of the image and facilitate more judicious decision-making across diverse applications.

Within this study, the classification process is conducted by leveraging the outcomes derived from processing X-ray data related to children's lungs. The aim is to differentiate between lungs afflicted with pneumonia and those without. The classification stages in this research employ a Support Vector Machine (SVM) for its discriminative prowess in distinguishing patterns within complex datasets.








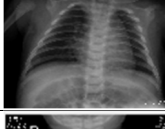


### III. RESULT AND DISCUSSION

This chapter elucidates the outcomes of the research conducted and processed in preceding stages, encompassing data collection, grouping of pediatric lung X-ray data, and data input. The input data undergoes systematic processing through various stages to yield results pertinent to this research. These include the findings from the pre-processing stage, outcomes of the segmentation stage, and results of the texture extraction stage utilizing the GLCM matrix.

#### 1) Data Collection and Data Grouping

These images were derived from X-ray examinations of pediatric lungs, specifically identifying cases of pneumonia and various other lung diseases. In this study we use 60 Lung X-Ray images from children. For sample data we show the dataset for testing comprised 7 instances of patients diagnosed with pneumonia and 3 patients instances of patients diagnosed with non-pneumonia with the total testing image is 10 images. The X-ray images of children's lungs, serving as the primary and input data, are presented in Table I below:

TABLE I. DATA COLLECTION

Patient Data	Children's Lung X-ray Image	Patient Data	Children's Lung X-ray Image
Patient 1 Pneumonia		Patient 6 Pneumonia	
Patient 2 Pneumonia		Patient 7 Pneumonia	
Patient 3 Pneumonia		Patient 8 Pneumonia	
Patient 4 Pneumonia		Patient 9 Pneumonia	
Patient 5 Pneumonia		Patient 10 Pneumonia	



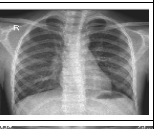

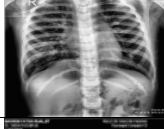













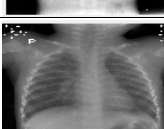






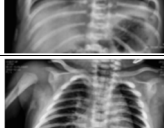

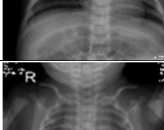

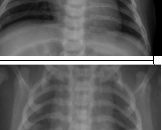
#### 2) Pre-Processing

The outcomes of testing X-ray images of pediatric lungs in the preprocessing stage commence with the input of the original image acquired from the SIEMENS MULTI SELECT DR X-ray machine. Subsequently, the original X-ray image undergoes transformation into a grayscale image. The subsequent phase involves the enhancement of the resulting grayscale image. Following enhancement, the subsequent stage entails image cropping. The image cropping process is executed through an automated system (auto-crop) to procure

an image object tailored to the specific requirements for further processing in subsequent stages.

The primary objective of these enhancements is to mitigate noise within the image. Following the enhancement, the subsequent step encompasses an image cropping process. The image cropping stage is executed to obtain an object with pixel values suitable for subsequent calculations, aligning with the specific criteria of the research. The test results from several stages can be seen in Table II below:

TABLE II. PRE PROCESSING RESULT

Patient No	RGB to Grayscale Result	Enhancement Result	Cropping Result
Patient 1 Pneumonia			
Patient 2 Pneumonia			
Patient 3 Pneumonia			
Patient 4 Pneumonia			
Patient 5 Pneumonia			
Patient 6 Pneumonia			
Patient 7 Pneumonia			
Patient 8 Non-Pneumonia			
Patient 9 Non-Pneumonia			
Patient 10 Non-Pneumonia			

The outcomes presented in Table II above represent the sequential stages of pixel transformation, transitioning from


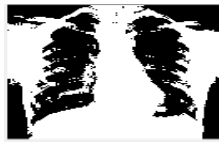












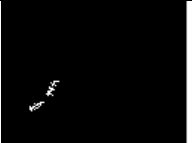
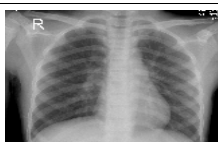
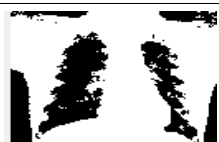














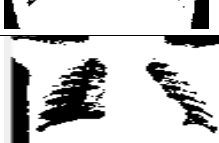




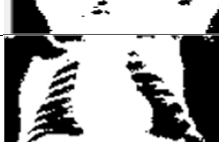



RGB to grayscale, followed by enhancement and cropping. Within the enhancement stage, a noticeable distinction is observed from the preceding phase, involving heightened contrast to elucidate image details and diminish noise, thereby enhancing overall results. The conclusive step in the preprocessing sequence is cropping. The cropping methodology in this research employs automated cutting based on predefined coordinates (Auto-cropping). The objective of cropping is to accentuate the primary object. The results of image testing at the preprocessing stage will undergo further processing to serve as input for the subsequent segmentation stage.

### 3) Segmentation

The cropping outcomes, executed in the preprocessing stage, lead to the subsequent segmentation stage. Within this

segmentation stage, multiple methods are employed, including multi-otsu thresholding, binary area opening, and segmentation. These steps are systematically implemented to obtain outcomes utilizing multi-otsu thresholding. The results derived from multi-otsu thresholding progress to the subsequent stage, namely binary area opening, the procedural details of which are documented in Table III. Following this, the succeeding phase involves image inversion, and the process details for acquiring image inversion results are delineated in Table III. The testing processes conducted in the segmentation stage, initiated from the cropping results and extending to multi-otsu thresholding, image inversion, and segmentation stages, are comprehensively documented in Table III below.

TABLE III. PROCESSING RESULT

Patient No	Cropping Result	Otsu Multi Thresholding	Binary Area Opening	Image Inversion	Image Segmentation
Patient 1 Pneumonia					
Patient 2 Pneumonia					
Patient 3 Pneumonia					
Patient 4 Pneumonia					
Patient 5 Pneumonia					
Patient 6 Pneumonia					
Patient 7 Pneumonia					
Patient 8 Non Pneumonia					



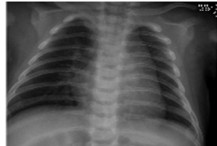









Patient No	Cropping Result	Otsu Multi Thresholding	Binary Area Opening	Image Inversion	Image Segmentation
Patient 9 Non Pneumonia					
Patient 10 Non Pneumonia					

Image testing is derived from the cropping outcomes and progresses to the multi-otsu thresholding stage. Multi-otsu thresholding is applied to determine threshold values exceeding two levels, aiming to ascertain the optimal threshold value for pixels. This approach is crucial as the research entails categorizing images into two classes based on the intensity value of each feature. Subsequently, an opening operation is employed to eliminate residual small objects persisting from the multi-otsu thresholding stage. Post-opening operation, the testing process involves transforming the image into a negative representation, facilitating the visibility of minute objects in the X-ray results.

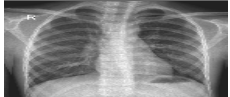
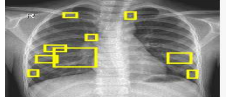
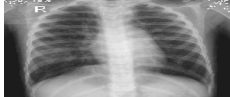

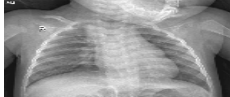

#### 4) Extraction Result

The texture extraction to be examined in this research utilizes the outcomes of prior image processing conducted at the segmentation stage. During the segmentation stage, an isolated image of the object is acquired, distinct from the background image. Subsequently, these segmentation results undergo processing utilizing the Gray Level Co-Occurrence Matrix (GLCM) matrix. The computations and assessments conducted involve the calculation of contrast, correlation, energy and homogeneity for each test image. The image extraction result is shown in Table IV below:

TABLE IV. EXTRACTION RESULT

Patient No	Contrast	Correlation	Energy	Homogeneity
Patient 1 Pneumonia	376.3859	0.95156	0.00020405	0.20544
Patient 2 Pneumonia	82.0856	0.99039	0.0012485	0.39256
Patient 3 Pneumonia	218.3247	0.97546	0.0025606	0.30254
Patient 4 Pneumonia	83.4468	0.98984	0.0037427	0.3507

TABLE V. CLASSIFICATION RESULT

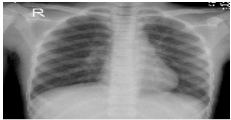
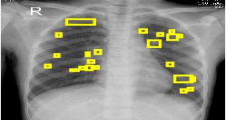

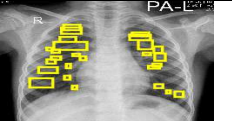

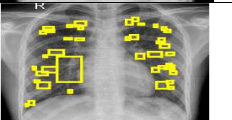

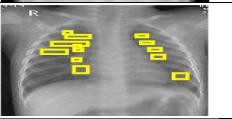


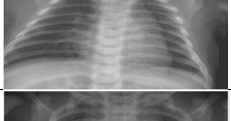
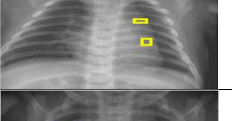
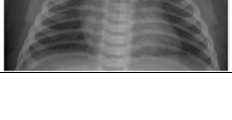
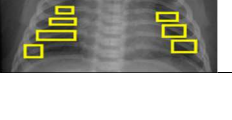
Patient No	X-ray Image	Object Detection	Number of Pixels	Classification
Patient 1 Pneumonia			10235	Pneumonia
Patient 2 Pneumonia			10473	Pneumonia
Patient 3 Pneumonia			2760	Pneumonia

Patient No	Contrast	Correlation	Energy	Homogeneity
Patient 5 Pneumonia	167.0495	0.9822	0.005773	0.30456
Patient 6 Pneumonia	53.408	0.99309	0.00085873	0.32461
Patient 7 Pneumonia	79.9901	0.98661	0.00045782	0.37829
Patient 8 Non Pneumonia	44.0604	0.99254	0.000524328	0.36124
Patient 9 No Pneumonia	129.8115	0.97732	0.00033508	0.30456
Patient 10 No Pneumonia	71.769	0.985	0.00022888	0.26541

Based on Table IV above, the calculated values for each GLCM matrix are obtained. Contrast, Correlation, Energy and Homogeneity values which is obtained from each test image which is calculated using a basic formula based on calculations taken from the basic formula. The results of the GLCM values in table IV will determine the classification results of the input lung x-ray image.

#### 5) Classification: Support Vector Machine (SVM)

The outcomes of the texture extraction, whose values have been computed through the Gray Level Co-Occurrence Matrix (GLCM), will subsequently undergo processing to categorize the test images into two result groups: images identified as pneumonia (non-pneumonia). The grouping of images for testing at the classification stage is executed utilizing the Support Vector Machine (SVM). The results of the testing in the classification stages are presented in Table V below:

Patient No	X-ray Image	Object Detection	Number of Pixels	Classification
Patient 4 Pneumonia			25427	Pneumonia
Patient 5 Pneumonia			33322	Pneumonia
Patient 6 Pneumonia			91056	Pneumonia
Patient 7 Pneumonia			15552	Pneumonia
Patient 8 Non Pneumonia			0	Non Pneumonia
Patient 9 Non Pneumonia			957	Non Pneumonia
Patient 10 Non Pneumonia			5384	Non Pneumonia

Analyzing the data presented in Table 5 above allows for the observation of test results categorizing images into those identified as pneumonia and those not identified as pneumonia. In instances where pneumonia is identified, the infected lung region is visibly demarcated with a yellow box, enabling the computation of pixel values within the marked area. Conversely, in images where pneumonia is not identified, the absence of discernible infected lung objects is evident, with the image results displaying no white spots on the lungs and pixels, totaling 0, 957, and 5384. The research results were obtained using 60 lung X-Ray images. From the 60 lung X-Ray images, 30 lung X-Ray images is pneumonia, and 30 lung X-Ray images not pneumonia. To calculate accuracy, we use the formula TP (true positive), TN (true negative), FP (false positive), and FN (false negative). Before we calculate the accuracy value, we will present the results of pneumonia detection in chest X-Ray images using the TP-TN-FP-FN matrix. Below is the matrix in question.

TABLE VI. MATRIX TP-TN-FP-FN

	Predictive Positive	Predictive Negative
Actual Positive	28	2
Actual Negative	1	29

To calculate the accuracy of this research we use is formula 1:

$$Accuracy = \frac{TP+TN}{TP+TN+FP+FN} \quad (1)$$

$$Accuracy = \frac{28+29}{28+29+2+1} = \frac{57}{60} = 0,95$$

So, the percentage of accuracy in this research is  $0.95 \times 100\% = 95\%$ .

#### IV. CONCLUSION

The outcomes of the segmentation process lead to the subsequent extraction stage, focusing on the texture values derived from the segmented results. Specifically, this research emphasizes the enhancement of the Gray-Level Co-Occurrence Matrix (GLCM) formula. Each stage carried out in this research can run well. All input images utilized as training data were systematically archived with the requisite features. Additionally, all test images conducted in the pre-processing stage were successfully completed. From the research results were obtained using 60 lung X-Ray images. X-ray images of children as test data, This study were successful in detecting 28 true positive (TP) lung X-Ray images and 29 true negative (TN) images. Meanwhile, the results of false negative (FN) detection were 2 images and false positive (FP) were 1 images, so the accuracy in this study was 95%.

#### REFERENCES

- [1] S. Xiao, Z. Zhang, Y. Zhang, dan C. Yu, "Multipurpose Watermarking Algorithm for Medical Images," *Sci. Program.*, vol. 2020, 2020, doi: 10.1155/2020/8848885.
- [2] L. Chang, W. Ma, Y. Jin, dan L. Xu, "An Image Decomposition Fusion Method for Medical Images," *Math. Probl. Eng.*, vol. 2020, 2020, doi: 10.1155/2020/4513183.
- [3] I. Ahmed, M. Ahmad, dan G. Jeon, "Integrating Digital Twins and Deep Learning for Medical Image Analysis in the era of COVID-19," *Virtual Real. Intell. Hardw.*, vol. 4, no. 4, pp. 292–305, 2022, doi: 10.1016/j.vrih.2022.03.002.
- [4] Y. Luo dan L. Sun, "Digital subtraction angiography image segmentation based on multiscale Hessian matrix applied to medical diagnosis and clinical nursing of coronary stenting patients," *J.*

- Radiat. Res. Appl. Sci.*, vol. 16, no. 3, pp. 100603, 2023, doi: 10.1016/j.jrras.2023.100603.
- [5] M. teymoori dan K. Pourshamsian, "A new method in the production of protective sheets against X-ray radiation," *Heliyon*, vol. 10, no. 1, pp. e23301, 2024, doi: 10.1016/j.heliyon.2023.e23301.
  - [6] S. Choi *et al.*, "Photoacoustics X-ray free-electron laser induced acoustic microscopy ( XFELAM )," *Photoacoustics*, vol. 35, pp. 100587, 2024, doi: 10.1016/j.pacs.2024.100587.
  - [7] J. T. Parker, T. Dreier, D. Nilsson, dan S. A. Mäkiharju, "In-lab X-ray particle velocimetry for multiphase flows : Design principles and demonstration of O ( 1 kHz ) XPV," *Flow Meas. Instrum.*, vol. 96, no. October 2023, pp. 102536, 2024, doi: 10.1016/j.flowmeasinst.2024.102536.
  - [8] N. J. Hartley *et al.*, "Results in Physics Confirming X-ray parametric down conversion by time – energy correlation," *Results Phys.*, vol. 57, no. September 2023, pp. 107328, 2024, doi: 10.1016/j.rinp.2024.107328.
  - [9] L. K. Lei Chai, Wei Yi, Reza Hoseinnezhad, "Jou rna IP pro of Jou pro of," *Rob. Auton. Syst.*, pp. 104136, 2022, doi: 10.1016/j.nima.2024.169078.
  - [10] G. Liyanage, M. Gonapaladeniya, dan T. Dissanayake, "Invasive Candidiasis Associated with Adenovirus Pneumonia," *Case Rep. Pediatr.*, vol. 2021, pp. 1–3, 2021, doi: 10.1155/2021/9905474.
  - [11] W. Du, X. Luo, dan M. Chen, "A Practical Deep Learning Model in Differentiating Pneumonia-Type Lung Carcinoma from Pneumonia on CT Images: ResNet Added with Attention Mechanism," *J. Oncol.*, vol. 2022, 2022, doi: 10.1155/2022/8906259.
  - [12] G. Liu, X. Jiang, X. Zeng, Y. Pan, dan H. Xu, "Analysis of Lymphocyte Subpopulations and Cytokines in COVID-19-Associated Pneumonia and Community-Acquired Pneumonia," *J. Immunol. Res.*, vol. 2021, no. November 2019, 2021, doi: 10.1155/2021/6657894.
  - [13] H. Mimouni *et al.*, "Spontaneous pneumomediastinum associated with covid-19 pneumonia," *Case Rep. Med.*, vol. 2020, pp. 17–19, 2020, doi: 10.1155/2020/4969486.
  - [14] C. Ter Chao, H. Y. Yeh, dan K. Y. Hung, "Chest radiography deep radiomics-enabled aortic arch calcification interpretation across different populations," *iScience*, vol. 26, no. 4, pp. 106429, 2023, doi: 10.1016/j.isci.2023.106429.
  - [15] H. Park *et al.*, "Feasibility of new patient dose management tool in digital radiography: Using clinical exposure index data of mobile chest radiography in a large university hospital," *Heliyon*, vol. 9, no. 10, pp. e20760, 2023, doi: 10.1016/j.heliyon.2023.e20760.
  - [16] T. Takaki, S. Murakami, N. Tani, dan T. Aoki, "Evaluation of the clinical utility of temporal subtraction using bone suppression processing in digital chest radiography," *Heliyon*, vol. 9, no. 1, pp. e13004, 2023, doi: 10.1016/j.heliyon.2023.e13004.
  - [17] F. Chutivanidchayakul, T. Suwatanapongched, dan T. Petnak, "Clinical and chest radiographic features of missed lung cancer and their association with patient outcomes," *Clin. Imaging*, vol. 99, no. December 2022, pp. 73–81, 2023, doi: 10.1016/j.clinimag.2023.03.017.
  - [18] H. Hiraiwa *et al.*, "Dynamic chest radiography as a novel minimally invasive hemodynamic imaging method in patients with heart failure," *Eur. J. Radiol.*, vol. 161, no. January, pp. 110729, 2023, doi: 10.1016/j.ejrad.2023.110729.
  - [19] M. Masud *et al.*, "A Pneumonia Diagnosis Scheme Based on Hybrid Features Extracted from Chest Radiographs Using an Ensemble Learning Algorithm," *J. Healthc. Eng.*, vol. 2021, 2021, doi: 10.1155/2021/8862089.
  - [20] N. Barakat, M. Awad, dan B. A. Abu-Nabah, "A machine learning approach on chest X-rays for pediatric pneumonia detection," *Digit. Heal.*, vol. 9, 2023, doi: 10.1177/20552076231180008.
  - [21] M. Yunianto, A. Suparmi, C. Cari, dan T. D. Ardyanto, "Gray Level Co-Occurrence Matrices and Support Vector Machine for Improved Lung Cancer Detection," *Int. J. online Biomed. Eng.*, vol. 19, no. 5, pp. 129–145, 2023, doi: 10.3991/ijoe.v19i05.35665.
  - [22] H. Sumarti, Q. Sabrina, D. Triana, F. Septiani, dan T. P. D. Rahmani, "Identification of COVID-19 Based on Features Texture Histogram and Gray Level Co-Occurrence Matrix (GLCM) Using K-Means Clustering Methods in Chest X-Ray Digital Images," *J. Penelit. Fis. dan Apl.*, vol. 13, no. 1, pp. 51–66, 2022, doi: 10.26740/jpfa.v13n1.p51-66.
  - [23] P. W. Adi, F. A. Nugroho, dan Y. P. Astuti, "New Image Texture Feature for Chest X-Ray Classification," *J. Appl. Intell. Syst.*, vol. 7, no. 1, pp. 8–15, 2022, doi: 10.33633/jais.v7i1.5340.
  - [24] H. Hendri *et al.*, "A hybrid data mining for predicting scholarship recipient students by combining K-means and C4.5 methods," *Indones. J. Electr. Eng. Comput. Sci.*, vol. 33, no. 3, pp. 1726, 2024, doi: 10.11591/ijeecs.v33.i3.pp1726-1735.
  - [25] H. Hendri, - Masriadi, dan - Mardison, "A Novel Algorithm for Monitoring Field Data Collection Officers of Indonesia's Central Statistics Agency (BPS) Using Web-Based Digital Technology," *Int. J. Adv. Sci. Eng. Inf. Technol.*, vol. 13, no. 3, pp. 1154, 2023, doi: 10.18517/ijaseit.13.3.18302.
  - [26] G. W. Nurcahyo, A. P. Gusman, dan H. Hendri, "Literature Study on Online Learning as an Impact of Covid 19 Pandemic in Education," *Proc. - 2nd Int. Conf. Comput. Sci. Eng. Eff. Digit. World After Pandemic (EDWAP), IC2SE 2021*, pp. 1–5, 2021, doi: 10.1109/IC2SE52832.2021.9792065.
  - [27] A. Frisch-Niggemeyer, P. Weihs, M. Revesz, S. F. Schreier, dan A. Richter, "Relating atmospheric aerosol amounts to blue to red ratio and grayscale contrast fluctuations using digitalization of routine webcam photographs taken in the urban environment of Vienna," *Atmos. Environ.*, vol. 290, no. August, pp. 119345, 2022, doi: 10.1016/j.atmosenv.2022.119345.
  - [28] X. Yang, R. Guo, dan H. Li, "Comparison of multimodal RGB-thermal fusion techniques for exterior wall multi-defect detection," *J. Infrastruct. Intell. Resil.*, vol. 2, no. 2, pp. 100029, 2023, doi: 10.1016/j.iintel.2023.100029.
  - [29] F. Attivissimo, V. I. D'Alessandro, A. Di Nisio, G. Scarcelli, J. Schumacher, dan A. M. L. Lanzolla, "Performance evaluation of image processing algorithms for eye blinking detection," *Meas. J. Int. Meas. Confed.*, vol. 223, no. March, pp. 113767, 2023, doi: 10.1016/j.measurement.2023.113767.
  - [30] J. O. Healthcare Engineering, "Retracted: An Ensembled Spatial Enhancement Method for Image Enhancement in Healthcare," *J. Healthc. Eng.*, vol. 2023, pp. 9876909, 2023, doi: 10.1155/2023/9876909.
  - [31] T. T. Dündar, E. Cetinkaya, İ. Yurtsever, Ö. Uysal, dan A. Aralaşmak, "Follow-Up of High-Grade Glial Tumor; Differentiation of Posttreatment Enhancement and Tumoral Enhancement by DCE-MR Perfusion," *Contrast Media Mol. Imaging*, vol. 2022, 2022, doi: 10.1155/2022/6948422.